Biomedical Signal Processing and Control 88 (2024) 105616

Contents lists available at ScienceDirect

Biomedical Signal Processing and Control

journal homepage: www.elsevier.com/locate/bspc

Automated diagnostic classification of diabetic retinopathy with microvascular structure of fundus images using deep learning method

G. Sivapriya [a,*], R. Manjula Devi [b], P. Keerthika [c], V. Praveen [d]

[a] Department of ECE, Kongu Engineering College, Erode, India
[b] Department of CSE, KPR Institute of Engineering and Technology, Coimbatore, India
[c] School of Computer Science and Engineering, Vellore Institute of Technology, Vellore, India
[d] Department of CSE, Bannari Amman Institute of Technology, Sathyamangalam, India

ARTICLE INFO

Keywords:
Retinal vascular segmentation
Diabetic retinopathy
Regularized random walker
Residual blocks

ABSTRACT

Multi-class classification is a major concern in the research field, especially in medical image analysis. This work proposes a novel method for automatically segmenting the blood vessels and classifying Diabetic Retinopathy (DR) using fundus images. This system helps ophthalmologists with the early detection and grading of DR diseases. The main aim here is to detect any pathological changes happening in the retinal vascular structure for the development of DR, through which the patients can avoid undergoing expensive scans. The proposed system involves three different stages, including pre-processing, vessel segmentation, and classification. The input images are processed first to eliminate the noise, followed by green channel extraction and enhancement with Contrast Limited Adaptive Histogram Equalization (CLAHE) and gamma correction. Retinal Vascular Structure (RVS) segmentation is a major concern in this work as it is responsible for detecting the different stages of DR by detecting the presence of microaneurysms, haemorrhages, and exudates. The U-Net is used as a base architecture to develop the segmentation model. The contracting path in the U-Net contains four consecutive downsampling and upsampling layers with skip connections. After performing downsampling four times, information on the tiny blood vessels may be missed. Therefore, ResEAD2Net is introduced in this work, where the number of downsampling and upsampling layers is reduced to two instead of four, and two such contracting paths and expansion paths are added to the network. Thus, detailed semantic information can be retained with this structure. Residual blocks are included instead of convolution blocks to increase the computational speed. To include structural connectivity, the segmented output is passed through the proposed Regularized Random Walker (RRW) algorithm, which focuses on the broken blood vessels. Finally, the features are extracted from the vessel structure and passed through the Machine Learning (ML) classifier to predict the DR grading. The proposed method achieves better performance in segmentation with accuracy, sensitivity, specificity, and area under the curve values of 98.07%, 90.24%, 99.01%, and 97.51%, respectively, for the STARE dataset and 97.55, 90.07, 98.01, and 97.64, respectively, for the DRIVE dataset. It is also found that the features obtained from the segmentation and ML classifier outperforms the existing methods in multiclass classification by achieving accuracy, sensitivity, and specificity of 98.88%, 98.91%, and 98.29% with the Messidor-2 dataset.

1. Introduction

Diabetics is one of the chronic diseases that is characterised by a rise in blood sugar levels when the pancreas does not produce sufficient insulin. This can cause severe damage to the eyes, Retinal Blood Vessels (RBV), nerves, and heart [1]. Diabetes, if not detected and treated properly, can be a serious cause of permanent vision damage. Diabetes mellitus can directly cause DR, which causes blockage of blood vessels to the eye and can result in major eye injury. 2.2 billion people are affected by vision impairment, as reported in the 2019 World Health Organisation Report on Vision. Around 1 billion of them could have been cured if they had been treated earlier [2]. Abnormal growth of vessels in the retina is a prominent cause of DR, which results in bleeding and eventually causes blindness. DR can be classified into Proliferative Diabetic Retinopathy (PDR) and non-proliferative Diabetic Retinopathy (NPDR), where NPDR is again classified into mild, moderate, and severe. Mild

* Corresponding author.
E-mail address: gsivapriya21@gmail.com (G. Sivapriya).

https://doi.org/10.1016/j.bspc.2023.105616
Received 12 May 2023; Received in revised form 14 September 2023; Accepted 15 October 2023
Available online 21 October 2023

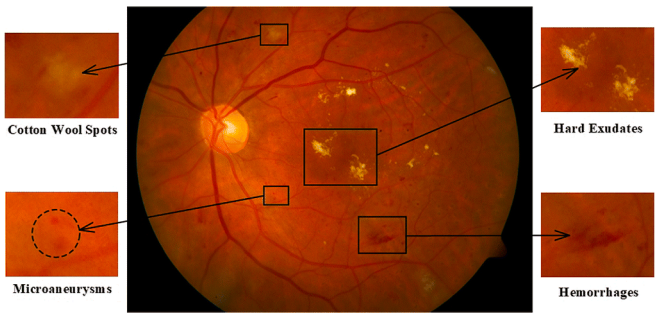

Fig. 1. Presence of MA, HE, Exudates.

NPDR: It is the starting stage of DR; the Blood Vessels (BV) are swollen as a small balloon-like structure in the eye, and it is known as microaneurysms (MA). Fluid leakage occurs because of the presence of MA. Moderate NPDR: MA causes leakage of blood in the retina due to the presence of Haemorrhages (HE) and Exudates (EX). Severe NPDR: Blood supply gets blocked in the retina, and this stage may also cause the development of new BV. PDR: In this stage, the new BV can cause leakage of blood, which makes the tissue contract and results in retinal detachment. Fig. 1 shows the presence of MA, HE, and exudates in the retinal fundus image [3].

Identification of these diseases manually consumes more time and is error-prone. The use of advanced image processing techniques makes the segmentation of RBV an easy task. From there, the DR severity level can be quickly classified. Thus, the implementation of computer-based systems assists the ophthalmologists in the fast screening of patients and avoids the need for several scans.

Many algorithms have been introduced in recent years to analyse and segment retinal fundus images. The algorithms are classified into two major categories: supervised and unsupervised learning models. Unsupervised models use contour methods to detect the blood vessels [4,5]. Morphological approaches [4,8], matched filter approaches [6,7], and deformable models [9,10] are preferred for vessel segmentation in unsupervised methods. Labelled Ground Truth (GT) is needed for training the supervised models. For this, publicly available datasets like CHASE, STARE, DRIVE, and MESSIDOR can be utilized. Many authors have used the Convolutional Neural Network (CNN) as a base model to classify vessel and non-vessel regions [30]. In the segmentation of blood vessels, there are much well-defined architecture, such as Alex-Net [11], U-Net [12], and the extension of U-Net for improving segmentation performance [13,14]. Most of the studies have achieved better segmentation performance, but still, there are many spaces for achieving the desired performance. Retinal structure contains vasculature, composed of numerous vessels connected like a tree with roots and branches. In different regions, RBV appears in low contrast with varying thickness. Several challenges could be faced while doing vessel segmentation, such as background noise, varying contrast, varying width of vessels, presence of MA, HE, and EX in different regions, shadows of the optic disc, and the closeness of two parallel blood vessels.

The contributions of the proposed work are:

1. Image quality is first enhanced with the pre-processing step to facilitate the deep learning models by eliminating background noise, contrast variation, uneven illumination, and the central reflection of light.
2. A deep learning method, ResEAD2Net (a variant of the U-Net model), is proposed to preserve the spatial and spectral domain features.
3. Regularized Random Walker (RRW) is proposed to link the broken blood vessels. It takes the output of ResEAD2Net and vessel directions to perform a regularized walk.
4. Sixteen essential features like variance, mean, skewness, kurtosis, standard deviation, contrast, entropy, energy, correlation, homogeneity, perimeter, area, eccentricity, convex area, filled area, and solidity are extracted and given to a Machine Learning-based Random Forest (MLRF) classifier.
5. The proposed method is validated against different existing methods with various performance measures.

The work is organised as follows: Section 2 explains the existing works in the area of segmenting retinal vessels and DR grading. Section 3 describes the overall proposed block, including pre-processing, network for vessel segmentation, vessel connectivity, and classification. Section 4 gives detailed information on the experimental results of the proposed work, and Section 5 describes the conclusion.

2. Related works

Lifeng Qiao et al. [15] given a solution for the prediction of DR and the inclusion of microaneurysms in the occlusion images. The newly recommended system examines the occlusion images for the presence of microaneurysms. The efficiency and certainty of NPDR identification are improved using the diabetic retinopathy system. Xiaomeng Li et al. [16] proposed a new cross-disease attention network to identify the interrelationship between the diseases in DR and Diabetic Macular Edema (DME). The meaningful features of the individual diseases are learned through disease-specific attention modules. The evaluation is carried out with the help of two benchmark datasets, Messidor and the IDRiD challenge dataset. Eman et al. [17] given a method to identify and analyse different pathological variations accompanying DR improvement, and it provides a solution without feeding the sick people with expensive scans of the retina. At first, the noise is removed, and the difference between the healthy and DR cases is identified as a second one. The system extracts four modifications and six features, and eight benchmark datasets were utilized to prove the proposed method's performance. Meysam Tavakoli et al. [18] elaborated on the effects of the binary pre-processing types on retinal vessel segmentation types, which is the main objective of the presented study.

The segmentation steps are classified into a few types. The first one is smoothing, and the second type is enhancement. The third type is detection, and the fourth is localization. With the help of top-hat preprocessing, more than 80 % improvement was made in the segmentation methods. Josh Ignacio Orlando et al. [19] conducted a random field model to overcome the difficulty of the Potts model, which fails to deal with the elongated and thin structures. The available data sets are STARE, HRF, DRIVE, and CHASE_DB1, and the method is trained with respect to the state-of-the-art features. The outcome shows that the proposed method produces better outcomes in terms of F1-score, sensitivity, and G-mean. Khursheed Aurangazeb et al. [20] found modified particle swarm optimization method for retinal vessel segmentation, this improved the performance of both supervised and unsupervised learning models for CLAHE parameter tuning.

Sehrish Qummar et al. [21] proposed a classification solution for different stages of diabetic retinopathy. The Kaggle dataset was used and compared with the state-of-the-art approaches. This method identifies all the stages of diabetic retinopathy when compared to the currently available methods. Tahira Nazir et al. [22] suggested a solution for the different levels of diabetic retinopathy through the proposed tetragonal local octa pattern, and finally, it was classified with the help of an Extreme Learning Machine. The various datasets like Kaggle-DB, Drive, and STARE confirm that the proposed method produces a standalone solution when compared with the existing related approaches. Franklin et al. [23] proposed a solution to improve the accuracy of the segmentation algorithm. The method was tested with the DRIVE dataset. Red, green, and blue are the three primary color channels used as inputs to identify the retinal blood vessels. To update the weights in the feed-forward architecture, a back propagation algorithm is used. Jemima Jebaseeli et al. [24] used the CLAHE for pre-processing and the two-path convolutional network model for automatic feature vector generation and it produces better accuracy, sensitivity, and specificity than the

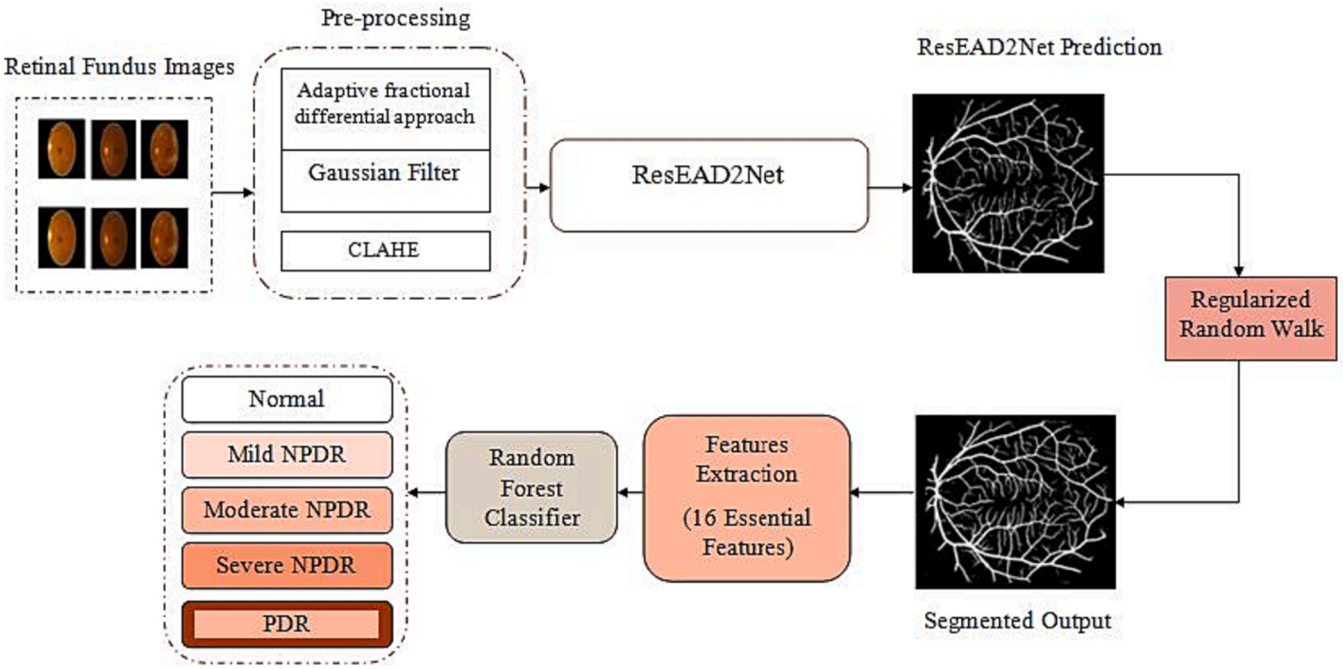

Fig. 2. The proposed system for segmenting the blood vessels and diagnosing DR grades with color fundus images.

standard public fundus image dataset.

3. Proposed method

ResEAD2Net is introduced in this work, which is inspired by the U-Net and Residual Net models. The work is proposed for classifying five different grades of DR (Normal, Mild NPDR, Moderate NPDR, Severe NPDR, and PDR). The detailed work flow of the proposed method is shown in Fig. 2. For the segmentation of RBV, ResEAD2Net and Regularized Random Walker are proposed in this paper. The classification of the DR grading is done here with segmented output of RBV. The input fundus images go through different pre-processing stages, including the adaptive fractional differential approach, gaussian filter, and CLAHE. It is further passed into the proposed ResEAD2Net and Regularized Random Walker to get the segmented image. ResEAD2Net, proposed in this work, is a hybridization of two encoding and decoding stages, deep residual block and channel attention block. Two encoding–decoding stages are adopted to extract the high-level semantic and edge features. This is done because the retinal blood vessels possess large changes in vessel curvature patterns. Encoding-decoding structure has proven to show promising outcomes in semantic segmentation tasks. Thus, the encoding–decoding method is chosen as the backbone of our proposed network. Deep Residual Blok is used to accelerate the convergence process of the algorithm and helps in solving the degradation problem by utilising the residual learning mechanism. To assure the structural connectivity of vessels, the RRW algorithm is proposed in this work based on graph theory. It takes the output of ResEAD2Net and vessel directions to perform a regularized walk. Finally, for multiclass classification (5 different DR gradings), 16 essential features are extracted and classified with the MLRF classifier.

3.1. Segmentation phase

A. Image Specific Pre-processing

Pre-processing the input image before applying it to the deep learning models helps the model learn quickly and produces better results. The contrast of BV is improved as the structure of BV helps in detecting a lot of eye-related diseases. From the RGB fundus image, the green channel is extracted as it has the most information related to the vessels and background. An adaptive differential approach [25] is used to increase the contrast of the image, preserving the background texture information.

Here, the vessels and other regions are processed individually. In the classical fractional differential approach, the higher-order function preserves the higher frequency information, and the lower-order function preserves the low frequency information. In an adaptive differential approach, the most optimal order is selected to provide the best contrast adjustment. Edge and texture information are essential to improving the contrast in the image. The G-L kernel is used to improve the image's edges and texture, and the Laplacian of Gaussian and standard deviation are used to improve the edge points and texture information from the vessel map. An averaging filter of size 3×3 is used for obtaining the 8-neighbourhood dependency of the vessel map structure. Averaging aids in the smoothing of edge and texture information as well as the removal of noise. The adaptive fractional differential operation is carried out with Equation (1).

$$q = \frac{1}{255}\left(\sum_{u=-1}^{1}\sum_{v=-1}^{1} a(u,v)*E_{LOG}(x+u,y+v) + \sum_{u=-1}^{1} \times \sum_{v=-1}^{1} a(u,v)*T_{UD}(x+u,y+v)\right) \quad (1)$$

a(u,v) is the averaging filter, $T_{UD}(x,y)$ is obtained by finding the standard deviation of neighborhood pixels, and $E_{LOG}(x,y)$ is the result of performing convolution operation between LOG operator and vessel map. The q value obtained from equation (1) is the optimal order and can be obtained by substituting in the value of K and convolving with the input image F(x,y) to obtain the enhanced image $F_{CE}(x,y)$ as given in equation (2).

$$F_{CE} = \sum_{u=-2}^{2}\sum_{v=-2}^{2} K(u,v)*F(x+u,y+v) \quad (2)$$

To increase the enhancement of thin blood vessels, a gaussian filter is applied to $F_{CE}(x,y)$ in the pre-processing stage. The kernel k(x,y) for the gaussian filter is given in equation (3).

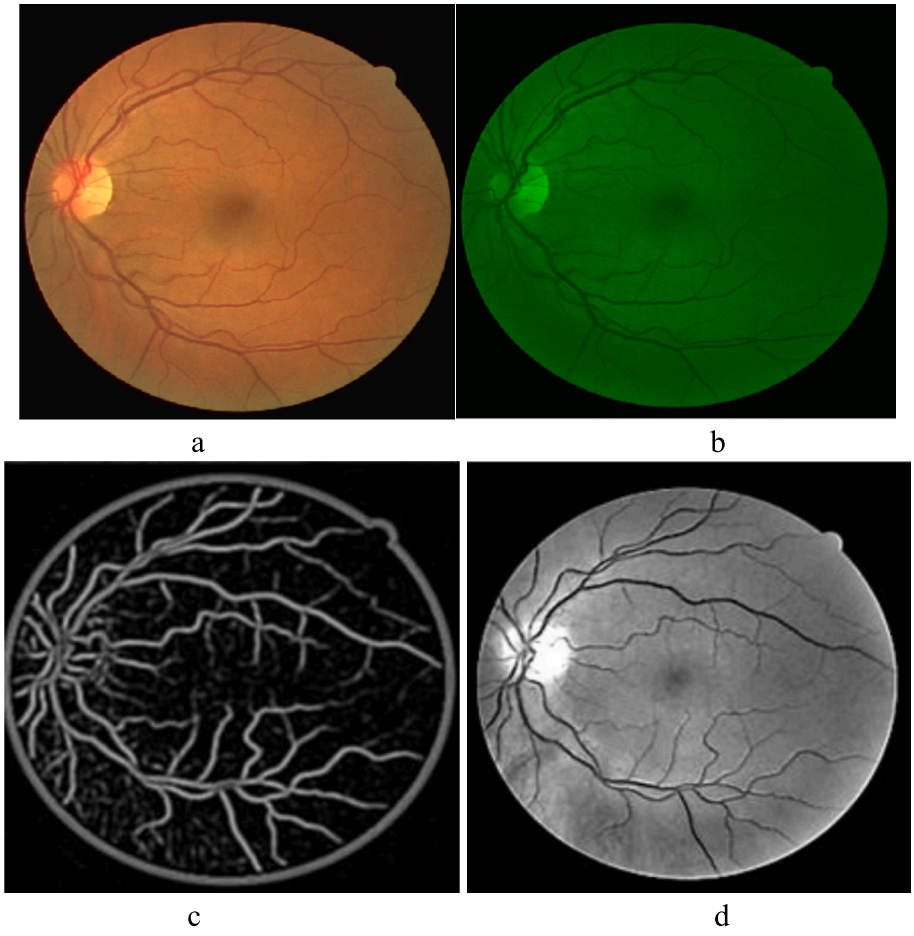

Fig. 3. A. Input fundus image, b. green channel, c. adaptive fractional differential approach, d. gaussian filter + CLAHE.

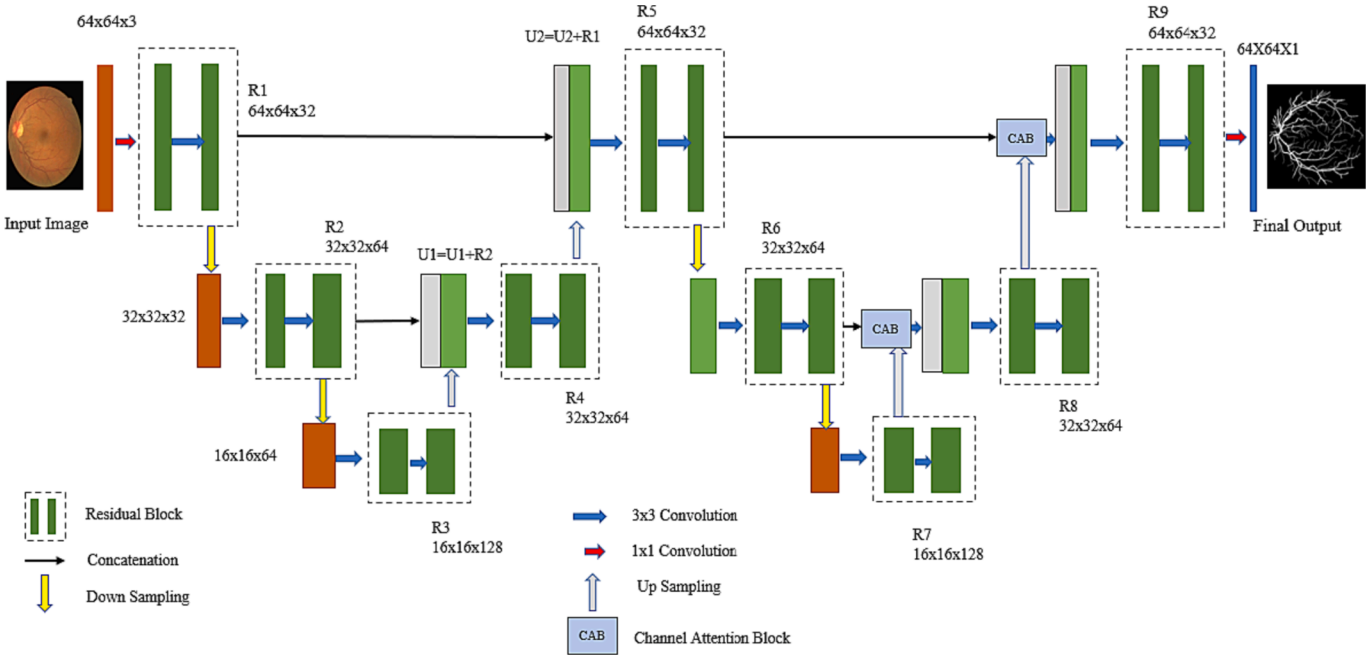

Fig. 4. Architecture of ResEAD2NET.

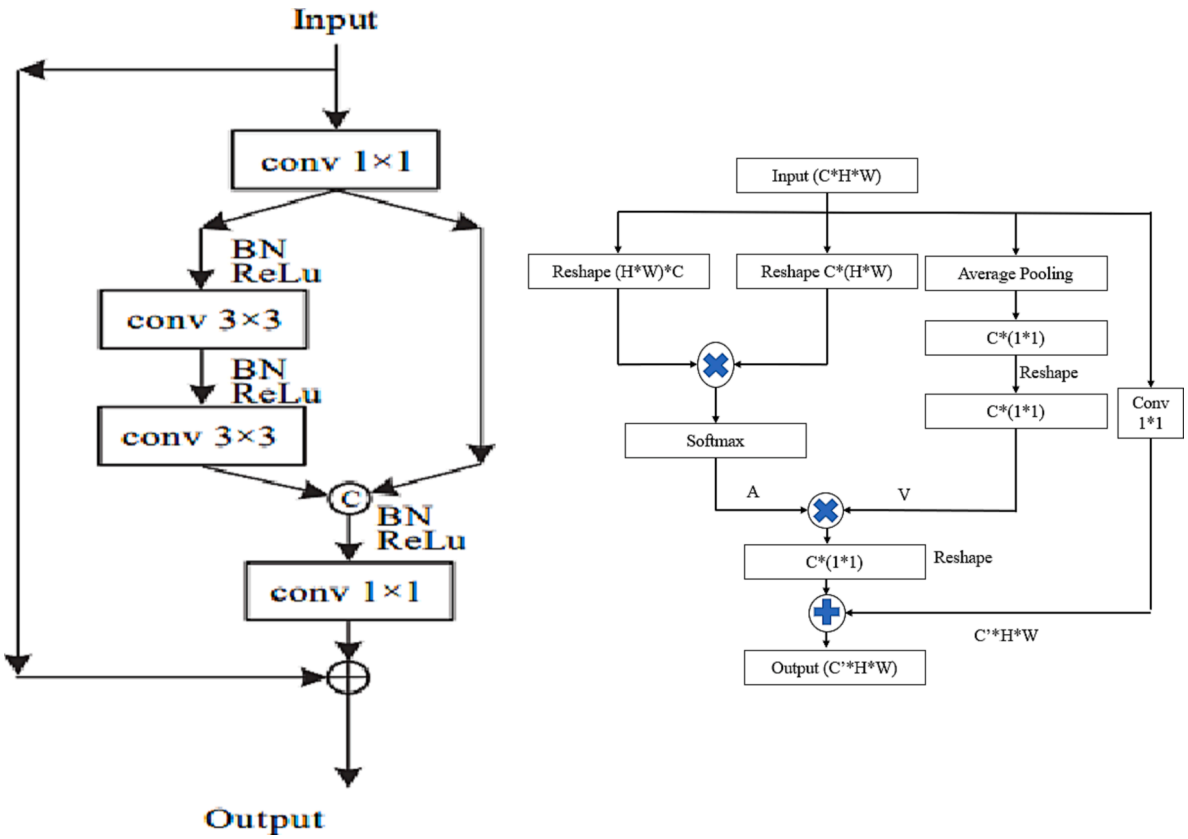

Fig. 5. a. Deep Residual Block, b. Channel Attention Block (CAB).

$$k(x,y) = -\exp\left(\frac{-x^2}{2\sigma^2}\right) |y| \le \frac{L}{2} \tag{3}$$

L, taken as the length of the vessel, σ is the variance that changes the variance of the intensity profile. The kernel k(x,y) is then convolved with the $F_{CE}(x,y)$, and the highest output response for every pixel is chosen. The value of L is chosen at 6 and σ as 0.5 for better visualisation of thin blood vessels. Finally, to improve the contrast, CLAHE is adopted, which distributes the brightness equally and avoids noise amplification. Here, a tile grid size of 8 and a clip limit of 0.02 are used. Fig. 3 shows the output image at each preprocessing stage.

ResEAD2Net

U-Net is generally preferred for biomedical image segmentation. As the skip connections are used from the encoder stage to the decoder stage, it helps in preserving all the low-level features and helps the classifier make appropriate decisions. Even after adding skip connections, as the network gets deeper, it carries more rich features than the low-level features containing the boundary and edge information. This causes a vanishing gradient problem in the training process of deeper networks. In addition, the U-Net variant continuously performs downsampling on the input fundus images four times, followed by upsampling. Four consecutive downsampling operations may lead to the loss of the most important features. Upsampling further cannot retrieve the lost information on thin vessel regions. Thus, the number of encoding and decoding paths is split into two. This modified U-Net named ResEAD2-Net is proposed and uses Deep Residual Block (DRB), Skip Connection, and Channel Attention Block (CAB) at the second decoding stage. The skip connection helps in fusing the lower and higher-level semantic features at the same level. The segmenting of smaller BV in the retinal fundus image is enhanced by fusing the lower and higher-level semantic features. The raw images are pre-processed and cropped to pxp as the input. Here, we consider p as 64, which is enough to retain sufficient information to segment the RBV. The image is passed to DRB, which contains different convolution operations with ReLu activation functions and maxpooling layers. The max pooling layer performs the downsampling operation to compress the feature size. The deconvolution layers that are present in the upsampling part of the architecture perform the unpooling operation, which is quite opposite to the pooling operation. The unpooling or upsampling operation is done to regain the actual activation obtained during the pooling operation. The output of the upsampling block is a probability map whose size matches the input image size. Skip connections are used to preserve the spatial information that is lost during the downsampling process. The skip connections are made from the upsampling part to the downsampling part, and this also helps in capturing the complete feature resolution. The structure of the proposed model is given in Fig. 4.

Deep Residual Block, the residual block with deep structure, introduced by [26], helps in solving the degradation issue and makes better optimisation of the network. U-Net is used as the base architecture, which consists of stacked residual blocks. As shown in Fig. 5.a, each block comprises four Conv layers (1×1, 3×3, 3×3, 1×1 filters), and each of these layers includes a batch normalisation and ReLu activation function. Two layers of 1×1 convolution blocks are added, one of which balances the parameters from two branches, and the other helps in reducing the dimension of the channels. In general, the residual network with identity mapping is expressed by equations (4) and (5).

$$y_p = h(x_p) + F(x_p, w_p) \tag{4}$$

$$x_{p+1} = f(y_p) \tag{5}$$

x_p and x_{p+1} represents the input and output of DRB, $h(x_p)$ denotes the skip connection, w_p is the parameter used in *pth* residual block. ReLu activation function is represented by f.

The DRB can be formulated by following equation (6) and (7)

$$H(x_p) = F(c(x_p), w_p) oc(x_p) \tag{6}$$

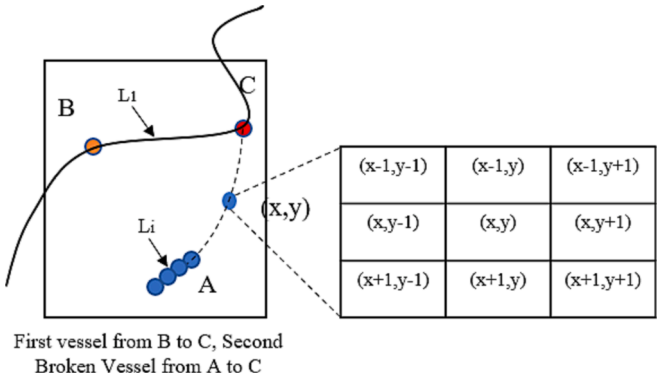

Fig. 6. Random Walker.

$$x_{p+1} = h(x_p) + c'(H(x_p), w_p') \tag{7}$$

Here o represents the addition operation where $H(x_p)$ represents its output. Among two 1 × 1 conv layer, first one is represented by c and second by c' which halves the feature dimensions. It is proven [27] that three 3 × 3 convolution layers produces better optimization results.

Channel Attention Block: Each channel contributes differently to various useful features. The dependencies of the channels are modelled by tuning the features so that the network will learn to improve the features that are contributing useful information and overwhelm the features that are not useful. CABs are added in the second stage of the decoder network to eliminate unnecessary and redundant information. Fig. 5.b shows the model structure of CAB. It further improves the interdependence between the channels.

The input $I \in \mathbb{R}^{C*H*W}$ is first reshaped into $K \in \mathbb{R}^{C*(H*W)}$ and $Q \in \mathbb{R}^{(H*W)*C}$. Then the resultant matrix K and Q are divided by $\sqrt{C}$ and softmax function is applied which is represented by $A \in \mathbb{R}^{C*C}$ and represented by the equation (8)

$$a_{ij} = Softmax\left(\frac{f(I_i, I_j)}{\sqrt{C}}\right) \tag{8}$$

a_{ij} represents the influence of the i^{th} channel on j^{th} channel and f for finding the relationship between i and j. Average pooling is applied to the original input $I \in \mathbb{R}^{C*H*W}$ for the reduction in dimension and to obtain the channel statistics. Matrix A and V are multiplied and reshaped into $\mathbb{R}^{C*1*1}$ and further multiplied by γ. The result is summed with the original input I to obtain the output $O \in \mathbb{R}^{C*H*W}$.

$$p(I_k) = \frac{1}{HXW} \sum_{i=1}^{H} \sum_{j=1}^{W} I_k(i,j) \tag{9}$$

Here p represents the average pooling, K = 1,2,…C, I = [i_1,i_2,…i_C].

$$O_j = \gamma \sum_{i=1}^{C} \left(a_{ij}.p(I_k)\right) + \omega_\theta I_j + b_\theta \tag{10}$$

γ is the learning parameter which starts from 0, ω_θ and b_θ represents the weight and bias for 1 × 1 Conv.

Equation (10) represents the final output of CAB which is the summation of average pooling with attention map and the features from the conv operation.

B. Regularized Random Walker (RRW)

Structural connectivity must be prioritised in the RVS task, which is overlooked in the majority of works that result in Broken Blood Vessels (BBV). BBV presents challenges in performing tasks like calculating the vessel length and detecting abnormal elongation of the vessels. Considering the above problem, this work uses graph theory and proposes a regularized random walker (RRW) for connecting the BBV. Fig. 6 depicts an example of the RRW algorithm, where the curve BC represents the normal vessel and the curve AC represents a broken vessel. Application of graph theory to random walks is used in [28] and [29] for semantic segmentation. Those methods were based on the neighbouring

Table 1
Features extracted from segmented fundus image and their mathematical expression.

S. No	Features Extracted	Formulae
	Mean (μ)	$\frac{1}{n}\sum_{i=1}^{n} x_i$
	Variance	$\frac{1}{n-1}\sum_{i=1}^{n}(x_i - x_1)^2$
	Standard Deviation	$\sqrt{Variance}$
	Entropy	$-\sum_{i=1}^{N} P_i log_2 P_i$
	Energy	$\sum_{i,j=1}^{N-1} P_{ij}^2$
	Contrast	$\sum_{i,j=0}^{N-1} P_{ij}^2 (i-j)^2$
	Correlation	$\sum_{i,j=0}^{N-1} \frac{(i-\mu_i)\left(j-\mu_j\right)}{\sqrt{(\sigma_i^2)(\sigma_j^2)}}$
	Homogeneity	$\sum_{i,j=0}^{N-1} \frac{P_{i,j}}{1+(i-j)2}$
	Area	$\sum_{i,j=0}^{M,N} b(i,j)$
	Perimeter	$\sum_{i,j=0}^{M,N} E_d(i,j)$
	Skewness	$\frac{\frac{1}{n}\sum_{i=1}^{n}(x_i - x_1^3)}{\sqrt{\left(\frac{1}{n}\sum_{i=1}^{n}(x_i - x_1)^2\right)^3}}$
	Kurtosis	$\frac{\frac{1}{n}\sum_{i=0}^{n}(x_i - x_1)^4}{\sqrt{\left(\frac{1}{n}\sum_{i=1}^{n}(x_i - x_1)^2\right)^4}}$
	Eccentricity	$\frac{1}{L_1}\sqrt{L_1^2 + L_2^2}$
	Convex Area	$\frac{1}{2}\left[\left(x_1.y_2 + x_2.y_3 + x_3.y_4 + \cdots + x_n.y_1\right) - \left(y_1.x_2 + y_2.x_3 + \cdots + y_n.x_1\right)\right]$
	Filled Area	$S^2 \subset R^3$
	Solidity	$\sum_{i=1}^{N_g}\sum_{j=1}^{N_g} \frac{1}{1+(i-j)^2} P(i,j)$

pixel's similarity. In deep learning, the probability of vessels and non-vessel regions is found and binarized with a threshold to get the segmented vessel output. Binarization might throw away some information, such as the variation between threshold and probability values. Inspired by this, RRW takes the probability outcomes of deep learning into the regularized walker. The probability of the pixels representing the foreground and background regions is taken into account for constructing the vessel map. The threshold value is normally set for distinguishing between foreground and background, and the same is utilised here for finding the probability. The structural connectivity obtained from ResEAD2Net is taken as a probability map for RRW. Let G=(V,E) represent the graph, where V is a set of vertices and E is a set of edges. Each pixel in the retinal image is considered a separate node in the graph; the similarity between the two pixels or nodes is computed based on the prediction output of ResEAD2Net.

L1 represents the large connected vessel, and Li represents the remaining components that need to be connected. Li is connected to L1 repeatedly until it reaches the final component.

Algorithm

Step 1: The minimum distance between two points is identified with the formula in equation (11).

$$d_{AB} = \text{argmin}\sqrt{(x_A - x_B)^2 + (y_A - y_B)^2} \tag{11}$$

Step 2: Region of interest is calculated for finding the broken vessel with the help of morphological operation (MATLAB Command: bwlabel).

Step 3: Correct direction of the vessel is calculated. Based on the finding, the missing points lie on the same curve of the left-over points (Li). Here second order polynomial equation is considered, where all the components in the Li try to fit in the curve ($y = ax^2 + bx + c$). The midway point between the curve and L1 is found as C (x_C, y_C).

Step 4: Initial walking points are calculated and moved iteratively until they reach L1. This walking procedure is optimized with the help of probability of the direction and Neural Network Probability (Pnn).

Walking direction is regularized with the equations from (12) to (14)

$$P(x^{'}, y^{'}) = \alpha P_d(x^{'}, y^{'}) + (1-\alpha) Pnn(x^{'}, y^{'}) \tag{12}$$

$P_d(x^{'}, y^{'})$ represents the relation between main direction and direction between current point to $(x^{'}, y^{'})$. $Pnn(x^{'}, y^{'})$ represents the probability that the point $(x^{'}, y^{'})$ is a vessel and it is taken from the output of proposed network where α is a trade-off value. $P_d(x^{'}, y^{'})$ and $P(x^{'}, y^{'})$ is calculated as

$$P_d(x^{'}, y^{'}) = \frac{1}{\sqrt{(x^{'} - xc)^2 + (y^{'} - yc)^2}} \tag{13}$$

$$(x^{'}, y^{'}) = \max\{P_d(x^{'}, y^{'})\} \max\{P_d(x^{'}, y^{'})\}, y^{'}) \in \Omega \tag{14}$$

Ω is the argument with 8 neighbourhoods of the current point (x,y). If Pnn is determined to be less than 0.1, the walking process may stop as it may not belong to the fractured region (Region of Interest). The probability will be less when the estimated point A is not the correct point for connection, and the process will be terminated to avoid the wrong connection.

3.2. Classification phase

Feature Extraction

The feature extraction phase is done to highlight certain properties of the image that are responsible for the necessary information for our task. The features extracted from the feature space should be capable of providing the necessary information required for the classifier. 16 distinct features, including textural, shape, and statistical features, are extracted, which are given in Table 1.

Gray Level Co-occurrence Matrix (GLCM) helps in calculating texture-based features and statistical features like contrast, correlation, entropy, homogeneity, mean, energy, variance, standard deviation, skewness, and kurtosis. Texture features describe certain useful information related to the region of interest. GLCM is the most widely used approach for finding texture features, and it gives information on pixel arrangement and its colour intensity levels in the image. Geometric information is extracted from shape-based features like area, perimeter, solidity, and eccentricity. Principle Component Analysis (PCA) is adopted to lessen the dimensions of the features.

Table 2
DR grading by the presence of lesions.

Severity Grade	Retinal Findings
0	Normal
1	Presence of MA's only
2	At least one HE or MA or one of the following
	Retinal HE
	Hard EX
	Cotton Wool Spots
	Venous beading
3	Any of the following
	Greater than 20 internal HE
	Venous beading
	Prominent IRMA
4	Neovascularization or pre-retinal HE

Table 3
Dataset size before and after data augmentation.

Dataset	Original Data Count	Augmented Data Count	Concatenated Data Count
DRIVE	40	3800	3840
STARE	20	1900	1920
CHASE_DB1	28	2660	2688
MESSIDOR-2			
Normal	1017	83	1100
Mild NPDR	269	831	1100
Moderate NPDR	343	757	1100
Severe NPDR	74	1026	1100
PDR	35	1065	1100

Table 4
Training Options.

Parameter	Value chosen
Optimization Algorithm	Adam [$\beta_1 = 0.9, \beta_1 = 0.99$]
Learning rate	0.001
Regularization	L2 Regularization
Initialization Technique	Xavier
Epochs	50
Loss Function	Cross Entropy

3.3. Random forest classifier

MLRF classifier is utilised in this work for the classification of DR grading. Five classes of labels are added as feature vectors. Random forest is a type of ensemble method that has a group of decision trees, each having an independent random vector [29]. Let K^{th} tree has a random vector as φ_k which is not dependent of earlier generated vectors $(\varphi_1, \varphi_2, \cdots \varphi_{k-1})$. The total number of trees set for classification is 100.

Pseudocode:

1. Features are selected randomly from the total available features (16 features are used in this work).
2. The best split method is adopted for finding the mother node.
3. Use the same method for splitting the other features into branches.
4. Loop steps 1–3 until the root node and the leaf node with branches are formed.
5. Iterate steps 1–4 for constructing the forest n times and create n trees.

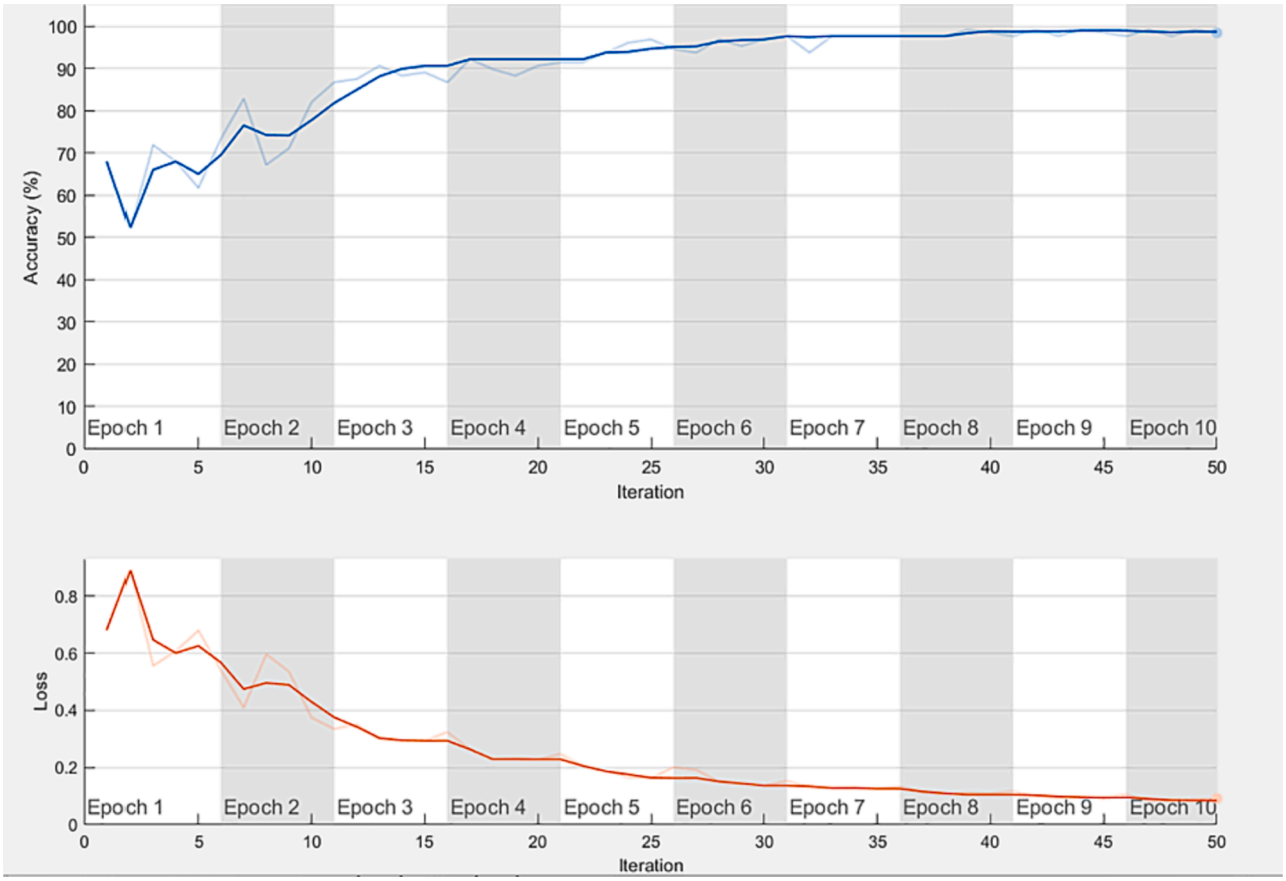

Fig. 7. Training accuracy and loss.

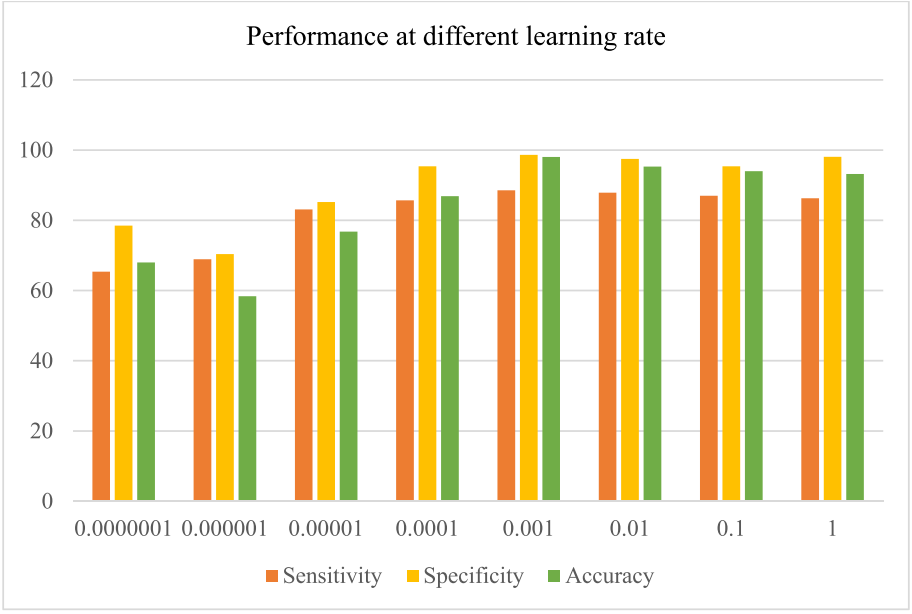

Fig. 8. Proposed model performance at various learning rate.

Table 5
Error generated by RRW at different values of α.

α	0	0.05	0.10	0.15	0.20	0.25	0.30	0.35	0.40	0.50
E_{rr}	0	0.1150	0.1035	0.0207	0.0195	0.0180	0.1060	0.1200	0.2350	0.2375

4. Experiments

A. Dataset Description

Drive dataset [31] comprises a total of 40 different fundus images captured while screening 400 diabetic patients between the ages of 25 and 90. Each image has a size of 565 × 584 pixels with two manually marked structures, where the first set is used as Ground Truth (GT). Seven of those 40 images have signs of mild DR. 40 images were divided into 20 for training and the rest 20 images for the testing phase. The STARE dataset contains 400 fundus images, but only 20 are used in this work as they have GT for vessel structure. Among the selected images, 10 were healthy, and the remaining 10 were found to have signs of DR. The dimensions of each image in this dataset are 700 × 605. Here, we have 15 images for training and 5 for testing. CHASE_DB1 contains a total of 28 images [32], which are segmented by two experts for GT. The first GT sets were taken for this experiment. The images were captured by 14 school children, and each one has a size of 999 × 960. 14 images were taken for training and the rest is for the testing phase from the CHASE_DB1. Table 2 gives information on the grading level and the presence of lesions in each grade.

The MESSIDOR-2 dataset is also used in this work, as they include images for different grades in DR. It contains a total of 1748 images, some of which are labelled incorrectly, and the final correct grading is done with 1738 images. It contains five different grading levels from 0 to 4 (Normal: 1017; Mild: 269; Moderate: 343; Severe: 74; and PDR: 35). For the training and testing process, the Messidor-2 dataset is divided into 80:20 ratios.

B. Evaluation Criteria

In order to evaluate the performance, we have utilised accuracy, sensitivity, specificity, and area under the receiver operating characteristic curve (ROC and AUC) as evaluation measures. [33] Sensitivity refers to the ability of the proposed method to predict the vessels correctly. Specificity is the ability in predicting the non-vessel regions correctly. Accuracy is the relationship between correctly segmented pixels and the total pixels. Precision describes the number of correct positive predictions. The Dice Score Coefficient (DSC) shows the resemblance between the predicted output and the GT. Intersection over Union (IoU) is the area covered by the union of the detected image and the ground truth image. The performance of proposed work is calculated

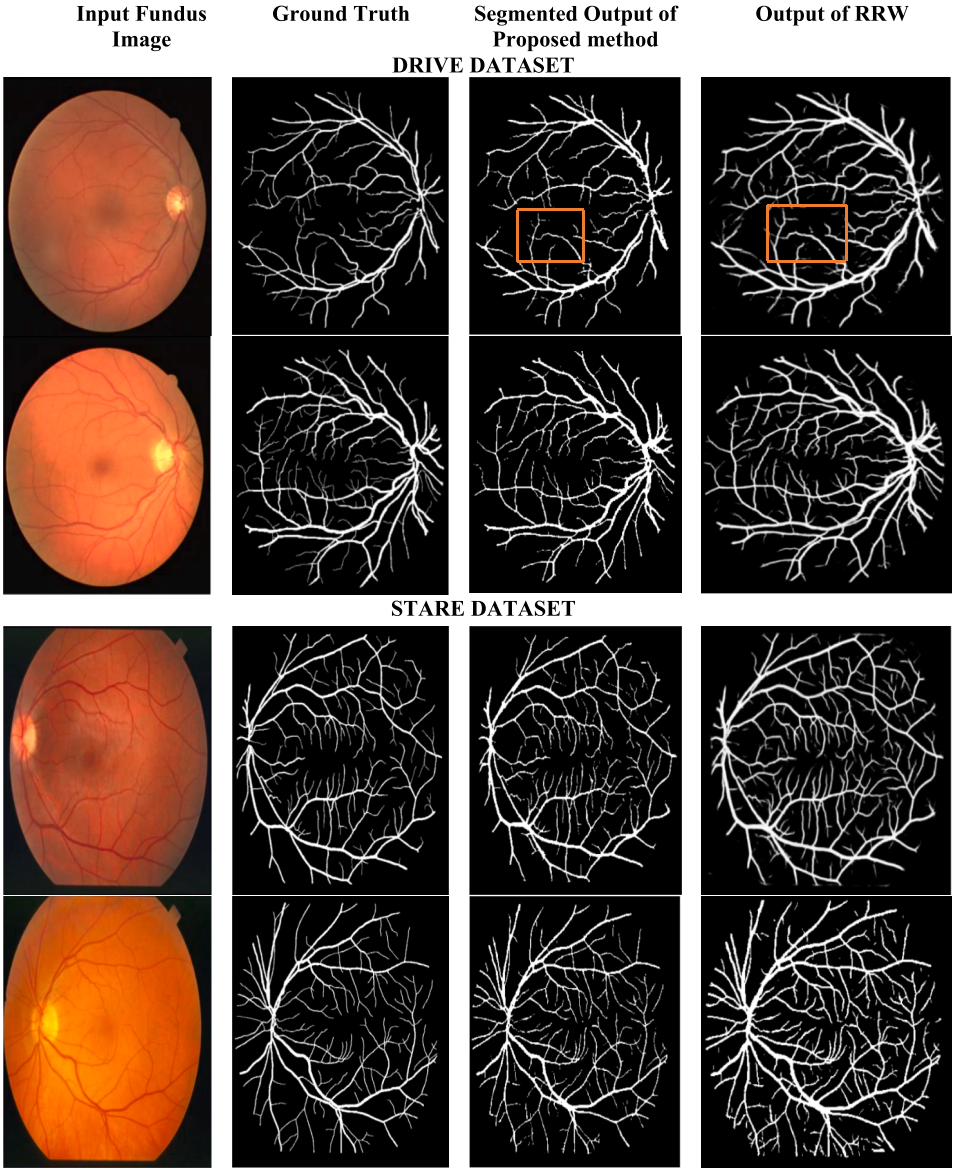

Fig. 9. Segmentation results obtained from DRIVE and STARE dataset.

Table 6
Performance of segmentation algorithm on DRIVE and STARE for each input image.

Image_ID	Sensitivity (%)		Specificity (%)		Accuracy (%)	
	DRIVE	STARE	DRIVE	STARE	DRIVE	STARE
1	89.97	91.05	98.90	98.90	97.47	98.11
2	98.48	82.85	97.64	98.49	98.11	96.92
3	95.12	86.81	97.11	99.90	96.22	99.31
4	98.72	88.54	98.24	98.21	98.29	97.22
5	92.80	96.73	97.57	98.33	97.40	97.60
6	89.25	90.26	94.22	97.98	97.47	96.75
7	90.57	84.59	97.85	99.33	97.68	98.41
8	86.71	77.35	97.38	99.15	96.68	96.85
9	91.04	94.56	98.32	99.83	97.09	99.50
10	88.00	86.00	97.08	99.26	98.32	97.06
11	92.91	90.76	98.49	99.96	97.65	99.72
12	85.54	95.68	98.34	99.88	97.57	99.29
13	90.06	94.53	97.48	99.11	96.21	98.47
14	85.97	94.44	98.77	99.11	97.83	98.34
15	82.58	91.58	98.86	98.56	96.67	97.50
16	93.75	89.27	98.46	96.33	98.34	94.90
17	90.74	98.07	98.22	99.32	97.90	98.13
18	85.81	96.80	99.18	99.97	98.18	99.97
19	90.70	88.25	99.05	99.94	97.78	99.42
20	82.59	86.75	99.08	98.60	98.18	97.90
Mean	**90.07**	**90.24**	**98.01**	**99.01**	**97.55**	**98.07**

Table 7
Performance of proposed segmentation algorithm with various datasets.

Dataset	Sensitivity (%)	Specificity (%)	Accuracy (%)	DSC	IoU
DRIVE	90.07	98.01	97.55	0.989	0.963
STARE	90.24	99.01	98.07	0.981	0.947
CHASE_DB1	85.41	98.92	98.5	0.981	0.946
Average Value	**88.57**	**98.64**	**98.04**	**0.983**	**0.952**

Table 8
Analysis of segmentation models for various epochs.

Database	DRIVE		STARE		CHASE_DB1	
Epochs	DSC	IoU	DSC	IoU	DSC	IoU
Epoch 1	0.971	0.952	0.958	0.937	0.956	0.911
Epoch 2	0.969	0.942	0.979	0.939	0.951	0.899
Epoch 3	0.967	0.931	0.958	0.937	0.957	0.937
Epoch 4	**0.989**	**0.963**	**0.981**	**0.947**	**0.981**	**0.946**
Epoch 5	0.947	0.912	0.948	0.929	0.963	0.941
Epoch 6	0.975	0.941	0.961	0.901	0.954	0.931
Epoch 7	0.963	0.952	0.968	0.949	0.951	0.939

with the equations (15) to (20).

$$Sensitivity(Recall) = \frac{TP}{TP + FN} \tag{15}$$

$$Specificity = \frac{TN}{TN + FP} \tag{16}$$

$$Accuracy = \frac{TP + TN}{TP + TN + FP + FN} \tag{17}$$

$$Precision = \frac{TP}{TP + FP} \tag{18}$$

$$IoU = \frac{TP}{TP + FP + FN} \tag{19}$$

$$DSC = \frac{2xTP}{2xTP + FP + FN} \tag{20}$$

TP is true positive, where the pixel is found as a vessel in the segmented image and GT; TN is true negative, where the pixel is correctly represented as a non-vessel in the segmentation output; FP and FN are the misclassifications in the segmented output where the vessel and non-vessel regions are wrongly interpreted. ROC is a plot between correctly classified vessels and non-vessels. The best ROC curve is when it approaches the left corner, which represents that the algorithm's performance is working better.

Performance of the proposed RRW in the ROI can be evaluated by the parameter Err. Err defines how well the vessels are reconnected

$$E_{rr(i)} = \frac{1}{N_r}\sum_{i=}^{N_r}\left(\frac{FP}{TP + FP}\right)$$

N_r represents the number of ROI, Err shows the i^{th} pixel error generated by RRW. The algorithm works better for lower values of Err.

C. Implementation Details

The proposed ResEAD2net is implemented in MATLAB R2021b with an Intel Core i7 CPU at 3.40 GHz, 16 GB of RAM, and an NVIDIA GeForce MX350 running on a 64-bit Windows operating system. Drive, STARE, CHASE_DB1, and Messidor-2 datasets are used in this work. DRIVE, CHASE_DB1, and STARE datasets are used in the segmentation task, and the Messidor-2 dataset is used for classification. There exists a class imbalance problem in the grading of diabetic retinopathy into five distinct classes. This class imbalance problem can be avoided by using data augmentation techniques, which help generate more examples for underrepresented classes. It takes only the original training dataset and makes a cost-effective approach to increasing the diversity and size of the training dataset. Data augmentation is carried out in which horizontal and vertical flipping is done to create 20 images in each flip. With 20 images from Drive, 60 images are created after flipping. Various X-Y translations (X = 5 and Y = -5, X = -5 and Y = 5 without flipping, X = 5 and Y = 0 with horizontal flipping, X = -10 and Y = 10 with vertical flipping, X = 10 and Y = 5 without flipping) are done, which produces 3,840 images, which is sufficient for training with the DRIVE dataset. A similar operation is carried out with the CHASE_DB1 and STARE datasets, resulting in 1920 and 2688 images, respectively, for training the proposed model. In the Messidor-2 dataset, the target count is set at 1100 for data augmentation in each class. The dataset used and its count before and after augmentation are mentioned in Table 3. Data augmentation is also a trick to increase the generalizability of the model by artificially augmenting the dataset by randomly distorting it, for instance, by rotating the image, shifting the pixel location, or flipping horizontally or vertically. This can increase the training dataset's size and make it more likely that new test data may have a close relationship with the training dataset. After pre-processed the images are resized to 64 × 64 before applying to the network. Table 4 gives the details of the training options chosen for this work.

Class imbalance also occurs in binary classification because of some unevenly distributed elements in foreground and background. Cross entropy loss function is preferred here in classification tasks. The learning rate is adjusted from 0.0000001 to 1, and it is found that the network produces the better results at 0.001. L2 regularization and Adam optimizer with $\beta_1 = 0.9, \beta_1 = 0.99$ is used. Regularization greatly helps in reducing the overfitting and underfitting of the data. It regularizes the parameters of the model and penalizes the coefficients. Coefficients are added with the linear regression model and it is tried to optimize the coefficient for minimizing the cost function. It is observed that the network has learnt well with 50 iterations and remains the at same level of learning. Fig. 7 shows the training accuracy and loss incurred in the proposed method. Fig. 8 shows the performance of the architecture at different learning rates.

As shown in the Table 5, the value of α is varied from 0 to 0.5 with 0.05 step size and observed the value of E_{rr} to find the best minimum

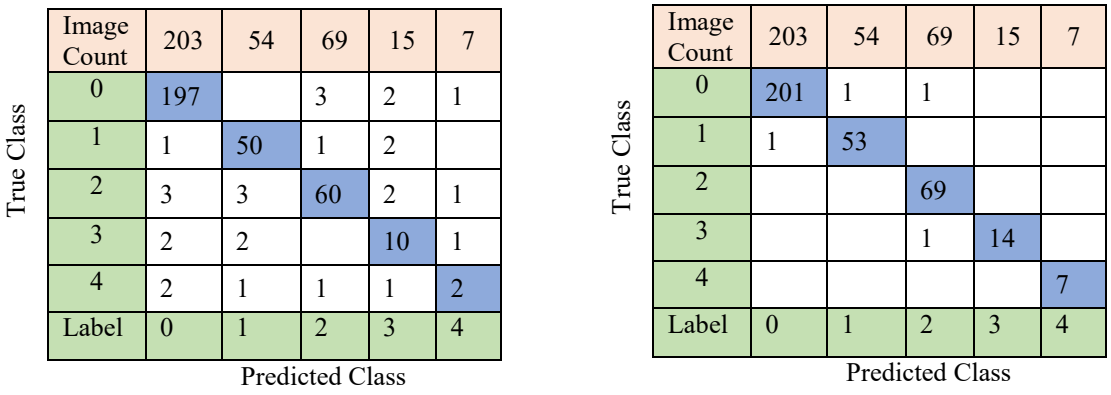

(0-Normal, 1-Mild, 2-Moderate, 3-Severe, 4- PDR)

Fig. 10. Confusion matrix obtained with a) Original Dataset b) Segmetation results of Proposed network.

Table 9
Results achieved after classification with MLRF.

Class	Sensitivity	Specificity	Precision	F-Score	Accuracy
Normal	99.9	97.85	98.32	98.2	100
Mild	97.6	97.35	98.06	98.1	98.9
Moderate	100	99.06	99.01	98.56	100
Severe	99.07	100	99.02	98.13	95.5
PDR	98	97.21	99.03	98.02	100
Overall	98.91	98.294	98.688	98.202	98.88

value. It is found that the error goes low at $\alpha = 0.25$. At initial position the walker takes larger probability to avoid escaping from initial position to L1. Same results are obtained for both DRIVE and CHASE_DB1 datasets.

D. Results and Discussion

In this work, the computation algorithms are utilised for the segmentation of RBV and the classification of DR from the fundus images. The output of the proposed ResEAD2Net architecture and RRW is given in Fig. 9. The input images are enhanced with the pre-processing techniques explained in Section 3.1 and fed as input to the architecture, which helps in segmenting the blood vessels. In literature, the CNN algorithm fails to detect the thin regions of BV surrounding the optic disc, which is overcome with the help of this double encoder decoder architecture. As there are still some fractured blood vessel regions, the RRW algorithm is applied to connect those broken blood vessels. The overall accuracy of 98.04 %, sensitivity of 88.57 %, and specificity of 98.64 % are obtained with the DRIVE, STARE, and CHASE_DB1 datasets, as shown in Table 7. It is proven that the proposed architecture works well by segmenting thin blood vessel regions. Double-encoding decoding stages in the architecture help in extracting semantic information from thin blood vessels and are further enhanced by residual and CAB's. Table 6 shows the performance of the architecture for the DRIVE and STARE datasets with 20 testing input fundus images from each. The segmented results are further utilised for the classification of DR grades from 0 to 4 with a random forest algorithm. The Messidor dataset is used here as it has five different grading levels.

The performance of the proposed segmentation model is also analysed in terms of training epochs for the selection of the best epoch for the dataset. The proposed model was trained with 50 epochs, but the focus is on the first 7 epochs, as they have shown notable improvements for the generated images. Table 8 shows the DSC and IoU values for the first 7 epochs for different datasets. From the table, we can observe that at some epochs, we get increased DSC and IoU, while in other cases, we get decreased DSC and IoU. It means that at few iterations, segmented output with more tiny vessels were generated with lower noise where at other iterations tiny vessels were missed.

Different classifiers were tested for DR grading, where the MLRF gave higher accuracy and sensitivity in classification. Fig. 10 shows the confusion matrix for classifying the diabetic retinopathy grading level with the original MESSIDOR dataset and with the segmented output of the proposed network. It is evident from Table 9 that the overall classification accuracy is 98.29 %, which is better when compared to the existing methods.

E. Comparison with state of art methods

To verify the performance of the proposed method, this section provides a comparison with existing methods. The proposed ResEAD2-Net is compared with the popular architectures SegNet and UNet[51]. SegNet for the RVS task is applied by Somo et al. (2017) [35]. U-Net became popular in the segmenting medical images [59], and it was applied to the RVS task by Lv et al. 2020 [36]. Many variations in the U-Net are proposed by various authors, including Lv et al. (2020)[36], who have introduced AA-UNet to overcome the uneven illumination caused by multiple layers in the U-Net. Table 10 provides a detailed comparison of various architectures with the DRIVE and STARE datasets. Fig. 12 shows that the AUC curve gradually increases and attains a stable state at 0.976. Therefore, the network performs well in segmenting the smaller blood vessel regions. The proposed method for multi class classification of DR is compared with other state of art methods in Table 11

Fig. 11 shows the comparison of segmentation outputs with state-of-the-art methods. As observed, the first and second columns show the input fundus image and GT images. The third column illustrates the output of a U-Net model, which has poorer segmentation results on tiny blood vessels, where the fourth column illustrates the output of DRIU [50], in which the vessel edges were not predicted accurately. The fifth column shows the output of the proposed model, where the tiny blood vessels are detected with reduced noise and produce more robust results.

F. Ablation studies

In the proposed model, ResEAD2Net and RRW are introduced to improve the efficiency of the baseline U-Net model. To justify the working efficiency of the proposed model, the following ablation study is done, where the DRIVE dataset is used for simplicity.

Table 10
Comparison of proposed method with the state-of-art segmentation networks.

Methods	Dataset	Accuracy	Sensitivity	Specificity	ROC_AUC
Zhang et al. (2017) [34]	**DRIVE**	94.63	78.95	97.01	–
Soomro et al (2017) [35]		94.6	74.6	91.7	83.1
Soomro et al. (2018) [37]		94.8	73.9	95.6	84.4
Wang et al. (2019) [13]		95.41	76.48	98.17	–
Jin et al. (2019) [12]		95.66	79.63	98.00	98.02
Guo et al. (2019) [38]		95.51	78.00	98.06	97.96
Khan et al. (2020) [39]		96.20	82.55	97.60	97.30
Kromm& Rohr, (2020) [40]		95.47	76.51	98.18	97.50
Park, K.B. et al (2020) [41]		83.46	83.46	83.02	–
Hu et. al. (2018) [42]		96.32	75.43	98.14	97.54
Yang, T et. al. (2020) [43]		95.60	83.40	98.20	97.86
Lv et al., (2020) [36]		95.54	78.49	98.02	97.77
Muhammad Arsalan et. al (2022) [48]		96.70	82.17	98.09	98.12
Proposed		***97.55***	***90.07***	***98.01***	***97.64***
Hajabdollahi et al., (2018) [44]	**STARE**	96.17	78.23	97.70	–
Yan & Yang (2018) [45]		96.38	77.35	98.57	98.33
Khan et al. (2020) [39]		96.23	83.18	97.58	97.58
Wang et al., (2019) [13]		95.38	79.14	97.22	97.04
Ramos-Soto, O et al (2021) [46]		95.8	74.74	98.36	–
Leopold et al., (2019) [47]		90.45	64.33	94.72	79.52
Arsalan et al., 2019 [33]		96.97	85.26	97.91	98.83
Oliveira, A et. al. (2018) [49]		96.94	83.15	98.88	99.05
Hu et. al. (2018) [42]		96.32	75.43	98.14	97.51
Guo et al. (2019) [38]		96.90	82.01	98.28	98.72
Feng et al., (2020) [50]		96.33	77.09	98.48	97.0
Proposed		***98.07***	***90.24***	***99.01***	***97.51***

Table 11
Performance comparison with state of art methods for multi class classification of DR.

Author (year)	Dataset	Method	Accuracy (%)	Sensitivity /Recall (%)	Specificity (%)
S. Gayathri (2020) [30]	Messidor	MultiLayer Perceptron	97.91	97.9	97.9
M. Nahiduzzaman et. al (2021) [52]	Messidor	CNN + ELM (Extreme Learning Machine)	96.26	94	98
E. Abdelmaksoud et. al. (2021) [53]	Messidor	UNet + SVM	92.1	92.9	91
Keerthiveena et. al., (2019) [54]	Messidor	WPT + SVM	96.3	95.8	97.8
M. Murugappan et. al., (2022) [55]	Messidor	ResNeXt	98.18	97.41	99.63
Xiang Li et. al (2022)[56]	Messidor	Pyramid Net	93.2	88.2	–
Proposed Method	Messidor	**ResEAD2Net + RRW + RF**	**98.88**	**98.91**	**98.29**
Lingling Fang (2022) [57]	DIARETDB1	DAG Network	98.7	–	–
Mahesh S Patil et., al., (2023) [58]	EyePACS	ResNet 50	97.87	–	–
T M Usman et., al., (2023) [60]	Kaggle	ResNet152	94.40	76.35	72.87
Tahira Nazir et. al., (2019) [22]	REVIEW-DB	Tetragonal Local Octa Patterns (T-LOP) + ELM	98.94	98.83	

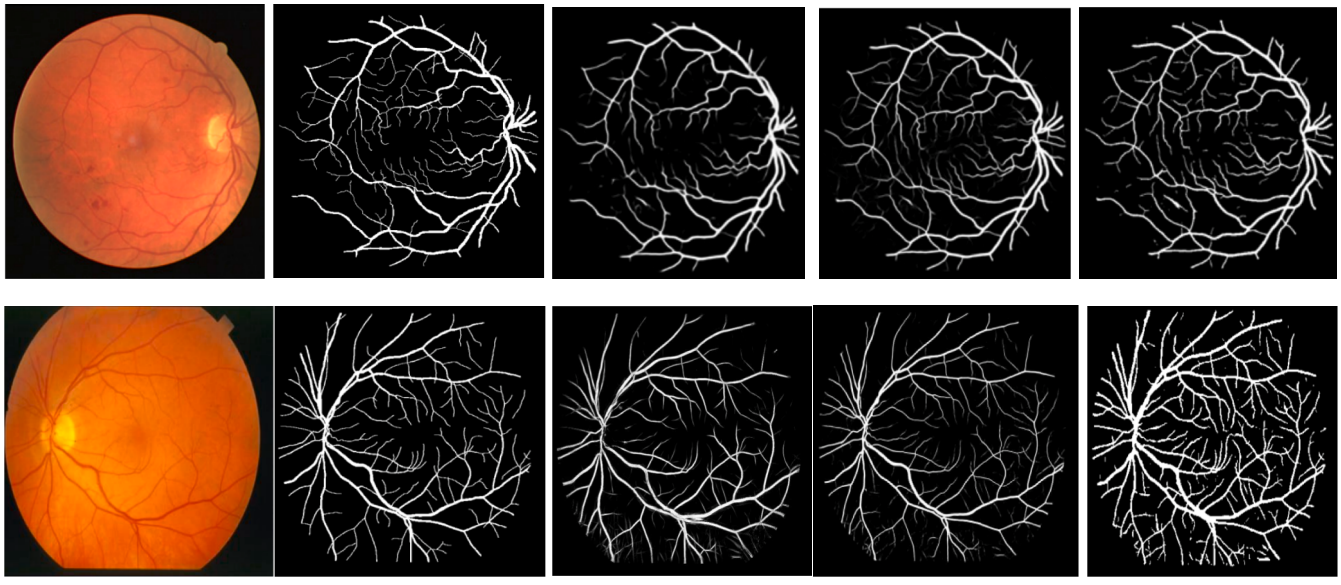

Fig. 11. Comparison of segmented outputs with state of art methods a) input fundus image b) GT image c) U-Net d) DRIU e) proposed method.

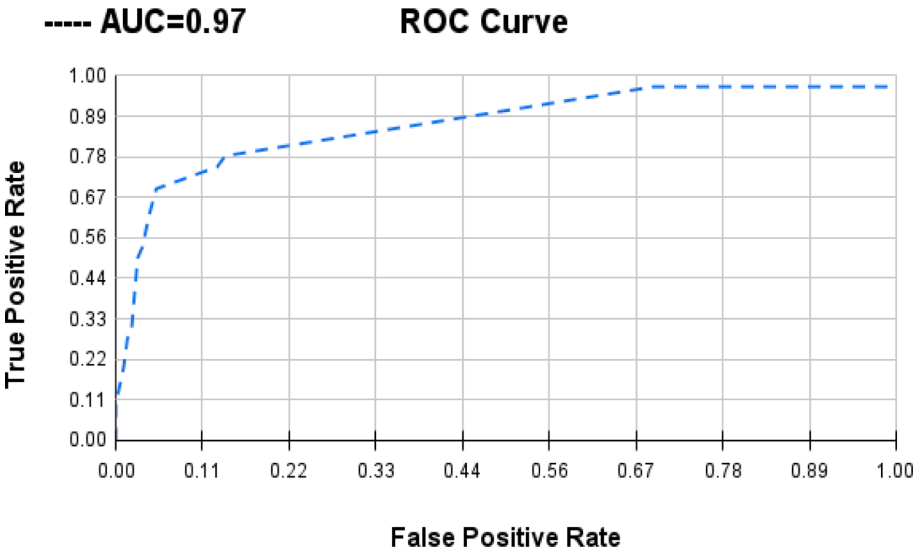

Fig. 12. ROC Curve.

Table 12
Ablation study for ResEAD2Net and RRW.

Method	Accuracy (%)	Sensitivity (%)	Specificity (%)
U-Net	94.8	73.9	95.6
ResEAD2Net	96.42	88.56	97.8
ResEAD2Net + ARWC	94.01	89.52	95.50
ResEAD2Net + RRW	97.55	90.07	98.01

1) *Ablation study for introducing two encoder decoder stages and replacing convolutional blocks with residual blocks:* The original U-Net model is replaced by a residual attention mechanism and two encoder-decoder stages. The segmentation results are compared with the other state-of-the-art methods in Table 10. This new method has achieved accuracy, sensitivity, and specificity of 97.55 %, 90.07 %, and 98.01 %, whereas the U-Net model proposed by U-Net [13] has produced 94.8 %, 73.9 %, and 95.6 % of accuracy, sensitivity, and specificity.
2) *Ablation study for regularized random walker:* To highlight the benefits of the proposed RRW, it is compared with Automatic Random Walks based on Centerlines (ARWC) [61]. Table 12 shows that the proposed model can produce higher values than ARWC. The results produced by RRW are comparatively higher than the existing ARWC model. The result without RRW is also given in Table 12. By adopting RRW, the accuracy, sensitivity, and specificity values are increased from 96.42 %, 88.56 %, and 97.8 % to 97.55 %, 90.07 %, and 98.01 %. This shows that RRW can effectively reconnect the broken blood vessels.

5. Conclusion

Segmentation of retinal blood vessels faces many challenges, like the presence of low-contrast micro-vessel structure, tiny vessels, pathologies, a reflex in the central vessel, and non-uniform illumination. It is still found to be an issue in medical image analysis. The human eye cannot view the micro-vessels, which can also be segmented with the help of the proposed ResEAD2Net architecture. Higher-level sematic features are extracted by applying the self-attention mechanism in the second decoder stage of the network, which improves interclass discernment and intraclass accumulation capabilities. It is proven that the shallow architecture can provide better information on the vessels to be segmented. The BBV regions can be correctly re-joined with the help of the RRW algorithm, which provides promising results. The illustration of the segmented outcomes is shown in Fig. 9. The proposed network is tested with three publicly available datasets (DRIVE, STARE, and CHASE_DB1). The work is further enhanced by adding the classification module, which includes MLRF for the grading of five different stages of DR. For multiclass classification, we have used all the categories (normal, mild, moderate, severe DR, and PDR) available in the MESSIDOR dataset. In order to validate the rigorous investigation of the work, there are lot of methods which are defined in the past and it is compared with the proposed methodology in Table 10 and it is proved that it outperforms all the methods with an accuracy of 97.55 %, 98.05 % on DRIVE and STARE datasets respectively. Overall classification accuracy of 98.29 % is achieved with the MESSIDOR dataset, which comprises five different classes. Although the best results as close to deep learning have been achieved using machine learning, our future work will focus on developing a robust deep learning algorithm for classification. The proposed work can be further extended to provide assistance for ophthalmologists by giving a second opinion on DR grading issues by analysing the real-time images.

CRediT authorship contribution statement

G. Sivapriya: Conceptualization, Data curation, Formal analysis, Methodology, Investigation. **R. Manjula Devi:** Formal analysis, Methodology, Investigation, Supervision. **P. Keerthika:** Supervision, Validation. **V. Praveen:** Validation, Writing - review & editing.

Declaration of Competing Interest

The authors declare that they have no known competing financial interests or personal relationships that could have appeared to influence the work reported in this paper.

Data availability

Data will be made available on request.

References

[1] World Health Organization, Diabetes. Accessed: Dec. 4, 2020. [Online]. Available: https://www.who.int/health-topics/diabetes#tab=tab_1.
[2] World Report on Vision, 2019.
[3] S. Long, J. Chen, A. Hu, et al., Microaneurysms detection in color fundus images using machine learning based on directional local contrast, BioMed. Engonline 19 (21) (2020), https://doi.org/10.1186/s12938-020-00766-3.

[4] F. Zana, J.-C. Klein, Segmentation of vessel-like patterns using mathematical morphology and curvature evaluation, IEEE Trans. Image Process. 10 (7) (2001) 1010–1019.

[5] L.C. Rodrigues, M.M. Marengoni, Segmentation of optic disc and blood vessels in retinal images using wavelets, mathematical morphology and Hessian-based multiscale filtering, Biomed. Signal Process Control 36 (2017) 39–49.

[6] S. Chaudhuri, S. Chatterjee, N. Katz, M. Nelson, M. Goldbaum, Detection of blood vessels in retinal images using two-dimensional matched filters, IEEE Trans. Med. Imaging 8 (3) (1989) 263–269.

[7] L. Gang, O. Chutatape, S.M. Krishnan, Detection and measurement of retinal vessels in fundus images using amplitude modified second-order Gaussian filter, I. E.E.E. Trans. Biomed. Eng. 49 (2002) 168–172.

[8] M.M. Fraz, A. Basit, S.A. Barman, Application of morphological bit planes in retinal blood vessel extraction, J. Digit. Imaging 26 (2) (2013) 274–286.

[9] T.B. Saha, D. Tchiotsop, R. Tchinda, G. Kenńe, Automated Extraction of the Intestinal Parasite in the Microscopic Images Using Active Contours and the Hough Transform, Current Med Imaging Rev. 11 (4) (2015) 233–246.

[10] Y. Zhao, L. Rada, K. Chen, S.P. Harding, Y. Zheng, Automated vessel segmentation using infinite perimeter active contour model with hybrid region information with application to retinal images, IEEE Trans. Med. Imaging 34 (9) (2015) 1797–1807.

[11] Z. Jiang, H. Zhang, Y.i. Wang, S.-B. Ko, Retinal blood vessel segmentation using fully convolutional network with transfer learning, Comput. Med. Imaging Graph. 68 (2018) 1–15.

[12] Q. Jin, Z. Meng, T.D. Pham, Q. Chen, L. Wei, R. Su, DUNet: a deformable network for retinal vessel segmentation, Knowledge Based Systems 178 (2019) 149–162.

[13] C. Wang, Z. Zhao, Q. Ren, Y. Xu, Y.i. Yu, Dense U-net based on patch-based learning for retinal vessel segmentation, Entropy 21 (2) (2019) 168.

[14] M.Z. Alom, M. Hasan, C. Yakopcic, T.M. Taha, V.K. Asari, Recurrent Residual Convolutional Neural Network Based on U-Net (R2U-Net) for Medical Image Segmentation, 2018.

[15] L. Qiao, Y. Zhu, H. Zhou, Diabetic Retinopathy Detection using Prognosis of Microaneurysm and Early Diagnosis System for Non - Proliferative Diabetic Retinopathy Based on Deep Learning Algorithms, IEEE Access 8 (2020) 104292–104302.

[16] Xiaomeng Li, Xiaowei Hu, Lequan Yu, Lei Zhu, Chi-Wing Fu, Pheng-Ann Heng, CANet: Cross-disease Attention Network for Joint Diabetic Retinopathy and Diabetic Macular Edema Grading, IEEE Trans. Medical Imaging (2019).

[17] E. Abdelmaksoud, S. El-Sappagh, S. Barakat, T. Abuhmed, M. Elmogy, Automatic Diabetic Retinopathy Grading System Based on Detecting Multiple Retinal Lesions, IEEE Access 9 (2021) 15939–15960.

[18] Meysam Tavakoli, Faraz Kalantari, Alireza Golestaneh, Comparing Different Pre-processing Methods in Automated Segmentation of Retinal Vasculature, IEEE, (2017).

[19] Jose Ignacio Orlando, Elena Prokofyeva, Matthew Blaschko, A Discriminatively Trained Fully Connected Conditional Random Field Model for Blood Vessel Segmentation in Fundus Images, IEEE Trans. Biomed. Eng. (2015).

[20] K. Aurangzeb, S. Aslam, M. Alhussein, R.A. Naqvi, M. Arsalan, S.I. Haider, Contrast Enhancement of Fundus Images by Employing Modified PSO for Improving the Performance of Deep Learning Models, IEEE Access 9 (2021) 47930–47945.

[21] S. Qummar, F.G. Khan, S. Shah, A. Khan, S. Shamshirband, Z.U. Rehman, I. Ahmed Khan, W. Jadoon, A Deep Learning Ensemble Approach for Diabetic Retinopathy Detection, IEEE Access 7 (2019) 150530–150539.

[22] T. Nazir, A. Irtaza, Z. Shabbir, A. Javed, U. Akram, M.T. Mahmood, Diabetic retinopathy detection through novel tetragonal local octa patterns and extreme learning machines, Artif. Intell. Med. 99 (2019) 101695.

[23] S.W. Franklin, S.E. Rajan, Computerized screening of diabetic retinopathy employing blood vessel segmentation in retinal images, Biocybernet. Biomed. Eng. 34 (2) (2014) 117–124.

[24] T.J. Jebaseeli, C.A.D. Durai, J.D. Peter, Segmentation of retinal blood vessels from ophthalmologic Diabetic Retinopathy images, Comput. Electr. Eng. 73 (2019) 245–258.

[25] S. Pearl Mary, V. Thanikaiselvan, Unified adaptive framework for contrast enhancement of blood vessels, Int. J. Electr. Comput. Eng. 10 (1) (2020) 767–777.

[26] K. He, X. Zhang, S. Ren, J. Sun, Deep residual learning for image recognition (2015).

[27] W. Liu, W.u. Guoqing, F. Ren, X. Kang, DFF-ResNet: An Insect Pest Recognition Model Based on Residual Networks, Big Data Mining and Analytics 3 (4) (2020) 300–310.

[28] Y. Yuan, C. Li, J. Kim, W. Cai, D.D. Feng, Reversion Correction and Regularized Random Walk Ranking for Saliency Detection, IEEE Trans. Image Process. 27 (3) (2018) 1311–1322.

[29] Lei Mou, Li Chen, Jun Cheng, Zaiwang Gu, Yitian Zhao, Jiang Liu, Dense Dilated Network with Probability Regularized Walk for Vessel Detection, arXiv: 1910.12010v1, (2019).

[30] S. Gayathri, P. Gopi Varun, P. Palanisamy, Automated classification of diabetic retinopathy through reliable feature selection, Phys Eng Science Med. (2019) 1–19.

[31] J. Staal, M.D. Abramoff, M. Niemeijer, M.A. Viergever, B. van Ginneken, Ridge-based vessel segmentation in color images of the retina, IEEE Trans. Med. Imaging 23 (4) (2004) 501–509.

[32] J.I. Orlando, E. Prokofyeva, et al., A Discriminatively Trained Fully Connected Conditional Random Field Model for Blood Vessel Segmentation in Fundus Images, IEEE Trans. Biomed. Eng. (2015).

[33] M. Arsalan, A. Haider, Y. Won Lee, K. Ryoung Park, Young Won Lee, Kang Ryoung Park, Detecting retinal vasculature as a key biomarker for deep Learning-based intelligent screening and analysis of diabetic and hypertensive retinopathy, Expert Syst. Appl. 200 (2022) 117009.

[34] J. Zhang, Y. Chen, E. Bekkers, M. Wang, B. Dashtbozorg, B.M.H. terRomeny, Retinal vessel delineation using a brain-inspired wavelet transform and random forest, Pattern Recogn. 69 (2019) 107–123.

[35] T.A. Soomro, A.J. Afifi, J. Gao, O. Hellwich, M.A.U. Khan, M. Paul, L. Zheng, Boosting sensitivity of a retinal vessel segmentation algorithm with convolutional neural network, In Proceeding of International Conference on Digital Image Computing: Techniques and Applications, NSW, (2017), 1–8.

[36] Y. Lv, H. Ma, J. Li, S. Liu, Attention Guided U-Net With Atrous Convolution for Accurate Retinal Vessels Segmentation, IEEE Access 8 (2020) 32826–32839.

[37] T.A. Soomro, O. Hellwich, A.J. Afifi, M. Paul, J. Gao, L. Zheng, Strided U-Net model: retinal vessels segmentation using dice loss, Proceedings of Digital Image Computing: Techniques and Applications (2018) 1–8.

[38] S. Guo, K. Wang, H. Kang, Y. Zhang, Y. Gao, T. Li, BTS-DSN: Deeply supervised neural network with short connections for retinal vessel segmentation, Int. J. Med. Inform. 126 (2019) 105–113, https://doi.org/10.1016/j.ijmedinf.2019.03.015.

[39] T.M. Khan, S.S. Naqvi, M. Arsalan, M.A. Khan, H.A. Khan, A. Haider, Exploiting residual edge information in deep fully convolutional neural networks for retinal vessel segmentation, in: Proceedings of International Joint Conference on Neural Networks, 2020, pp. 1–8.

[40] C. Kromm, K. Rohr, Inception capsule network for retinal blood vessel segmentation and centerline extraction, in: Proceedings of IEEE 17th International Symposium on Biomedical Imaging, pp. 1223–1226, 10.1109/ISBI45749.2020.9098538.

[41] K.B. Park, S.H. Choi, J.Y. Lee, M-gan: Retinal blood vessel segmentation by balancing losses through stacked deep fully convolutional networks, IEEE Access 8 (2020) 146308–146322.

[42] K. Hu, Z. Zhang, X. Niu, Y. Zhang, C. Cao, F. Xiao, X. Gao, Retinal vessel segmentation of color fundus images using multiscale convolutional neural network with an improved cross entropy loss function, Neurocomputing 309 (2018) 179–191.

[43] T. Yang, T. Wu, L. Li, et al., SUD-GAN: Deep Convolution Generative Adversarial Network Combined with Short Connection and Dense Block for Retinal Vessel Segmentation, J. Digit. Imaging 33 (2020) 946–957, https://doi.org/10.1007/s10278-020-00339-9.

[44] M. Hajabdollahi, R. Esfandiarpoor, K. Najarian, N. Karimi, S. Samavi, S. M. RezaSoroushmeh, Low complexity convolutional neural network for vessel segmentation in portable retinal diagnostic devices, in: Proceeding of 25th IEEE International Conference on Image Processing, Athens, 2018, pp. 2785–2789, https://doi.org/10.1109/ICIP.2018.8451665.

[45] Z. Yan, X. Yang, K.T. Cheng, A three-stage deep learning model for accurate retinal vessel segmentation, IEEE J. Biomed. Health Inform. (2018), https://doi.org/10.1109/JBHI.2018.2872813.

[46] O. Ramos-Soto, E. Rodríguez-Esparza, S.E. Balderas-Mata, D. Oliva, A.E. Hassanien, R.K. Meleppat, R.J. Zawadzki, An efficient retinal blood vessel segmentation in eye fundus images by using optimized top-hat and homomorphic filtering, Comput. Methods Programs Biomed. 201 (2021) 105949.

[47] H.A. Leopold, J. Orchard, J.S. Zelek, V. Lakshminarayanan, PixelBNN: Augmenting the PixelCNN with batch normalization and the presentation of a fast architecture for retinal vessel segmentation, J. Imaging 5 (2) (2019), https://doi.org/10.3390/jimaging5020026.

[48] M. Arsalan, M. Owais, T. Mahmood, S.W. Cho, K.R. Park, Aiding the diagnosis of diabetic and hypertensive retinopathy using artificial intelligence-based semantic segmentation, J. Clin. Med. 8 (9) (2019), https://doi.org/10.3390/jcm8091446.

[49] A. Oliveira, S. Pereira, C.A. Silva, Retinal vessel segmentation based on fully convolutional Neural networks, Expert Syst. Appl. 112 (2018) 229–242.

[50] S. Feng, Z. Zhuo, D. Pan, Q. Tian, CcNet: A cross-connected convolutional network for segmenting retinal vessels using multi-scale features, Neurocomputing 392 (2020) 268–276.

[51] KK Maninis, J Pont-Tuset, P Arbeláez, L Van Gool, Deep retinal image understanding, in: Proc. Int. Conf. Med. Image Comput. Comput.- Assist. Intervent., (2016), 140–148.

[52] M.D. Nahiduzzaman, et al., Hybrid CNN-SVD Based Prominent Feature Extraction and Selection for Grading Diabetic Retinopathy Using Extreme Learning Machine Algorithm, IEEE Access 9 (2021), https://doi.org/10.1109/ACCESS.2021.3125791.

[53] E. Abdelmaksoud, et al., Automatic Diabetic Retinopathy Grading System Based on Detecting Multiple Retinal Lesions, IEEE Access 9 (2021), https://doi.org/10.1109/ACCESS.2021.3052870.

[54] B. Keerthiveena, S. Esakkirajan, K. Selvakumar, T. Yogesh, Computer-aided diagnosis of retinal diseases using multidomain feature fusion, Int. J. Imaging Syst. Technol. (2019), https://doi.org/10.1002/ima.22379.

[55] M. Murugappan, et al., A novel few-shot classification framework for diabetic retinopathy detection and grading, Measurement 200 (15) (2022), 111485, https://doi.org/10.1016/j.measurement.2022.111485.

[56] X. Li, et al., Lesion-attention pyramid network for diabetic retinopathy grading, Artif. Intell. Med. 126 (2022), https://doi.org/10.1016/j.artmed.2022.102259.

[57] Lingling Fang, Huan Qiao, Diabetic retinopathy classification using a novel DAG network based on multi-feature of fundus images, 77 (2022), 10.1016/j.bspc.2022.103810.

[58] M.S. Patil, S. Chickerur, C. Abhimalya, A. Naik, N. Kumari, S. Maurya, Effective Deep Learning Data Augmentation Techniques for Diabetic Retinopathy Classification, Procedia Comput. Sci. 218 (2023) 1156–1165.

[59] G. Sivapriya, P. Keerthika, Computer aided diagnosis systems using deep learning for retinal diseases: A survey, Mater. Today Proc. 58 (Part 1) (2022) 286–292, https://doi.org/10.1016/j.matpr.2022.02.162.
[60] T.M. Usman, Y.K. Saheed, D. Ignace, A. Nsang, Diabetic retinopathy detection using principal component analysis multi-label feature extraction and classification, Int. J. Cognitive Comput. Eng. 4 (2023) 78–88.
[61] J. Gao, G. Chen, W. Lin, An Effective Retinal Blood Vessel Segmentation by Using Automatic Random Walks Based on Centerline Extraction, BioMed Research International 2020 (2020) 1–11.